

# First principle study of cobalt impurity in bcc Fe with Cu precipitates

N. I. Medvedeva · A. S. Murthy · V. L. Richards ·  
D. C. Van Aken · J. E. Medvedeva

Received: 30 May 2012 / Accepted: 7 September 2012  
© Springer Science+Business Media, LLC 2012

**Abstract** The addition of cobalt was experimentally observed to increase the strength and impact toughness of Cu precipitation hardened steel. In order to understand the mechanism of this strengthening, we studied the effect of cobalt in the bulks and surfaces of bcc Fe and bcc Cu, as well as at the Fe/Cu interface by ab initio density-functional approach. We investigated the cobalt distribution between the Fe matrix and Cu precipitate, and found that cobalt is rejected from the core of the Cu particle. The calculated elastic constants and stacking fault energies show that cobalt does not produce any solid solution softening or hardening in bcc Fe. However, cobalt segregated in the interfacial region increases the cleavage fracture energies and cleavage stress of the Fe/Co/Cu interface. The compressive stress, which arises near the interface due to strong Fe–Co bonds, may serve as a barrier for dislocation motion through the interface resulting in additional hardening.

## Introduction

The formation of nanometer-sized Cu precipitates in bcc Fe is important for attaining dispersion strengthening simultaneously with high ductility. The mechanism of Cu

strengthening effect is complicated and has been intensively studied [1–7]. Atomistic simulations were employed to investigate the effect of size, shape, composition, and structural instability of Cu particles on strengthening [2, 3, 7–15]. According to [2–7], precipitation strengthening was related to the dislocation pinning caused by the transformation of the unstable bcc structure to more stable Cu structures under shearing of Cu precipitates by dislocations (structural-transformation mechanism).

Recently, it was observed that cobalt addition improves the room temperature strength as well as the toughness of precipitation hardened steel; however, the mechanism of additional cobalt-induced strengthening was not established [16, 17]. In multi-component alloys, the effect of additions on the properties of precipitated steel strongly depends on their interaction with matrix and precipitate, as well as on the aging stages. Impurities may have a significant effect on the kinetics of Cu precipitation [18] and serve as nucleating centers for the precipitated phase or, vice versa, deplete the growth of precipitate. During aging, impurities are redistributed between the Fe matrix and Cu and they may move from the Cu core and segregate in the interface region (as Ni impurity) or their concentration may even increase in the Cu phase (as Mn impurity) at the intermediate stage of aging [19–22]. The segregated impurities forming the shell for the Cu particle may change the interfacial interaction and affect the dislocations running through the precipitate because the pinned dislocations are mainly located near the matrix/precipitate interface.

Possible reasons for additional hardening may involve chemical strengthening from the matrix–precipitate interface, as well as differences in stacking fault energies or shear moduli. In precipitated steel, solid solution hardening may occur along with precipitation hardening. It should be noted that there are contradictory results on the Co effect

---

N. I. Medvedeva (✉) · A. S. Murthy · V. L. Richards ·  
D. C. Van Aken  
Materials Science and Engineering, Missouri University  
of Science and Technology, Rolla, MO, USA  
e-mail: medvedeva@ihim.uran.ru

N. I. Medvedeva  
Institute of Solid State Chemistry, Yekaterinburg, Russia

J. E. Medvedeva  
Physics Department, Missouri University of Science  
and Technology, Rolla, MO, USA

on hardening in ferrite. Cobalt addition was experimentally found to result in alloy softening [23, 24], while no solid solution softening was observed in Fe–3 at.% Co between 77 and 295 K [25]. According to [26], neither softening nor hardening due to Co solute addition occurs at any temperature. Theoretical cluster calculations predicted that cobalt weakens the interatomic interactions in bcc Fe and results in solid solution softening [27].

The plasticity of bcc metals is governed by the  $1/2\langle 111 \rangle$  screw dislocations with a non-planar core. Ab initio approach based on the atomic row model [28–31] together with atomistic modeling predicted that core structure of the  $1/2\langle 111 \rangle$  screw dislocations in bcc Fe–Cu changes from non-polarized to polarized and the edge component is enhanced [32]. A similar trend in the transformation from isotropic to planar screw dislocation core under alloying was predicted in bcc Mo with softening solutes [29–31], where modeling of dislocation properties by the atomic row shift and by the planar slip gave similar results. The generalized stacking fault (GSF) energies [33], which describe the total energy changes under rigid sliding along the Burgers vector, have been demonstrated to be reliable and important characteristics for understanding of the solid solution behavior not only in fcc alloys [34] but also in bcc alloys with a non-planar core structure [29–31, 35].

In this paper, to understand the microscopic origin of Co effect, we employed a first principles density-functional method to investigate the Co partitioning between the Fe matrix and the Cu precipitate. First principles calculations are very useful for investigation of structure, stability, and thermodynamic properties of precipitates—see, for example [36]. The Cu precipitation during aging is known to follow the bcc Cu  $\rightarrow$  9R  $\rightarrow$  3R  $\rightarrow$  fcc Cu transformation. The Cu clusters less than 4–5 nm have a bcc structure and the peak hardness is reached when the bcc copper precipitates are still coherent with the Fe matrix [37–39]. For this reason, we used the bcc structure for Cu in the simulations of bulk, surface, and interface properties. We present results for the interaction between Cu and Co impurities in bulk as well as the mixing energies for Cu–Fe, Co–Fe, and Cu–Co alloys. Since the interfacial forces play an important role in the stabilization of bcc Cu precipitate and in the mobility of dislocations running through the interface, we study the cobalt effect on the geometry and bonding of the Fe/Cu interface and make conclusions about cobalt redistribution between the Fe matrix and bcc Cu. We are also interested in how the presence of iron in Cu particle affects cobalt distribution and study the possibility of cobalt segregation in the Fe matrix, Cu and at the Fe/Cu interface. We calculated the stacking fault energies for bcc solid solutions as well as the ideal cleavage energies and cleavage stress for the Fe/Cu and Fe/Co/Cu interfaces, and discuss the possible reasons for additional strengthening

due to cobalt impurity by comparing our theoretic predictions with the available experimental data on the cobalt effect on the Cu precipitate size, atomic distribution, and on the mechanical properties of Cu precipitation-hardened steel.

## Computational details

We employed the Vienna ab initio simulation package VASP in projector augmented waves pseudopotentials [40, 41] and the generalized gradient approximation (GGA) for the exchange and correlation effects [42]. We chose the kinetic energy cutoff of 350 eV and the number of  $k$ -points that gives correct lattice parameters for bulk Fe, Co, and Cu phases as well as the surface energy of Fe. All calculations were spin polarized. The atomic relaxation was performed by minimizing the Hellmann–Feynman forces up to 0.01 eV/Å over all atoms. For bcc Fe, our calculations gave the lattice parameter 2.836 Å and the magnetic moment  $2.21 \mu_B$  in good agreement with previous ab initio results (2.84 Å and  $2.20 \mu_B$ ) [43]. The lattice parameter for bcc Cu is equal to 2.889 Å, which is close to the ab initio value 2.873 Å [44] and to those calculated with empirical interatomic potentials (2.885 Å [45], 2.880 Å [14]). Calculations by the ab initio SIESTA method gave larger lattice parameters for both the bcc Fe (2.88 Å) and bcc Cu (2.91 Å) phases [46]. According to our calculations, the lattice misfit between bcc Fe and bcc Cu is 1.8 %, while EAM gave 0.45 % [15] and 3.2 % [47]. The SIESTA calculations provided misfit of 1 % [46]. We obtained the energy of strained bcc Cu relative to the equilibrium bcc Cu state of 16 meV/atom, which is close to 23 meV/atom obtained by Vitek and coworkers [48] and larger than that obtained from MD simulation (1 meV/atom) [15]. The energy difference between fcc and bcc Cu structures (8 meV/atom) is also larger as compared to the theoretic predictions (46 meV/atom [15], and from 7 to 48 meV/atom [2]). The optimized lattice parameters for hcp Co are  $a = 2.498 \text{ \AA}$ ,  $c/a = 1.614$ , and magnetic moment on Co atom is  $1.64 \mu_B$ .

## Results

### Additions in bulk bcc Fe and bcc Cu

#### Co and Cu clustering

To study the local Cu–Cu interaction in bcc Fe matrix, we considered a 54-atom cell ( $6 \times 6 \times 6$   $k$ -mesh) and compared the total energies of two Cu atoms at different substitutional sites including the first-nearest neighbors, the second-nearest neighbors, and the most distant positions in the supercell. We

found that the interaction between the first-nearest and between the second-nearest Cu atoms is strongly attractive. The energy gain estimated as the total energy difference relative to the distant Cu atom is +0.23 and +0.08 eV for the first- and second-nearest neighbor Cu atoms, respectively. The MD simulation [49] predicted +0.20 and +0.07 eV, while the SIESTA method yielded +0.15 and +0.03 eV for the Cu–Cu interactions in the first and second coordination shells, respectively [46]. The large interaction energy reflects a strong tendency of Cu atoms to clustering. Similar calculations for the two substituted Co atoms in the Fe supercell gave  $E_b$  of –0.03 and –0.09 eV for the first- and second-nearest neighbor Co atoms, respectively, with respect to the most distant positions of two Co atoms. This suggests that Co does not tend to segregate in Fe bulk.

Comparison of total energies for the first- and second-nearest neighbors with their distant positions for the Cu and Co atoms shows that their interaction is close to zero (<0.01 eV) and cobalt has no preference to occupy the nearest sites to Cu. Further, the estimations of interaction between the first- and second-nearest neighbor Co atoms relative to their distant sites in bcc Cu show attractive interactions with the energies 0.28 and 0.16 eV, respectively, which are even stronger than the Cu–Cu interactions in bcc Fe.

Taking into account the attractive Co–Co interaction in bcc Cu and the large positive mixing energy of Co–Cu (see below), it is possible to expect the formation of small Co clusters or Co couples in bcc Cu precipitate. In order to elucidate the role of chemical and magnetic interactions in the formation of Co clusters, we performed both spin-polarized and non-magnetic calculations for Co<sub>2</sub>, Co<sub>3</sub>, Co<sub>4</sub>, and Co<sub>9</sub> clusters in a 54-atom bcc Cu supercell. We found that magnetic moment on cobalt increases with the number of cobalt atoms in cluster from zero in Cu<sub>53</sub>Co to 1.35  $\mu_B$  in Cu<sub>52</sub>Co<sub>2</sub> and to 1.82  $\mu_B$  in Cu<sub>45</sub>Co<sub>9</sub>. In spin-polarized calculations we obtained that the configuration with the two nearest Co atoms forming a strong couple with the Co–Co distance of 2.322 Å is by 0.11 and 0.28 eV more stable than that with the second-nearest Co atoms ( $R_{Co-Co} = 2.714$  Å) or that with their most distant positions, respectively, whereas the non-magnetic calculations yielded the configuration with the second-nearest Co atoms to be by 0.07 eV more preferable than their nearest sites. A supercell with a Co cluster consisting of three nearest Co atoms has energy, which is by 0.52 eV lower than that with three most distant Co atoms. Thus, magnetism has an important effect on the stability of these clusters and the preference for magnetic cobalt clusters increases with the size of cluster.

### Mixing energies

We calculated the mixing energies for bcc Cu–Fe, Co–Fe, and Co–Cu solid solutions as a difference in the total energies

of the alloy and elemental metals in their stable states. There is a large difference in mixing energies for Cu–Fe and Co–Fe. For 1.8 at.% concentration of Cu and Co in bcc Fe (one impurity atom in 54-atom cell of bcc Fe), we obtained the mixing energies of +0.56 eV (previous estimations predicted close values from +0.48 to +0.55 eV, see [46].) and –0.14 eV, respectively, which correlates with the low solubility of Cu in bcc Fe and with the existence of continuous bcc Fe–Co solid solutions up to 80 at.% Co. The low solubility of Cu in bcc Fe along with the strong attractive Cu–Cu interaction favors the formation of copper precipitates. The mixing energies of 1.8 at.% Fe and 1.8 at.% Co in unstrained bcc Cu ( $a = 2.889$  Å) are +0.21 and +0.49 eV, respectively, and the obtained positive values correspond to a limited solubility of both Fe and Co in fcc Cu. The larger mixing energy for Co–Cu indicates that the Co impurity in bcc Cu is less favorable than the presence of Fe. This difference in mixing energies is explained by the electronic mechanism discussed below based on a comparison of the densities of Co 3d states in Co–Fe and Co–Cu alloys.

### Elastic properties

Finally, we established that cobalt has a little effect on the elastic moduli of bcc Fe, which is in agreement with the previous prediction [50]. We obtained  $C_{11} = 246$  GPa,  $C_{12} = 144$  GPa,  $C_{44} = 122$  GPa for pure bcc Fe (in good agreement with previous theoretic predictions and with experiment:  $C_{11} = 232$  GPa,  $C_{12} = 136$  GPa,  $C_{44} = 117$  GPa) [51] and  $C_{11} = 261$  GPa,  $C_{12} = 136$  GPa,  $C_{44} = 101$  GPa for bcc Fe–6 at.% Co. Using these elastic constants, we estimated the bulk modulus, which is calculated as  $B = (C_{11} + 2C_{12})/3$  for a cubic single crystal, and obtained  $B = 178$  GPa for both clean Fe and Fe–6 at.% Co. However, the single-crystal approximation for shear modulus  $G = (C_{11} - C_{12})/2$  gives  $G = 51$  GPa for bcc Fe, which is much smaller than the experimental value (82 GPa) and demonstrates the growth up to 63 GPa with addition of 6 at.% Co. We estimated the Young's modulus along  $\langle 100 \rangle$  and  $\langle 111 \rangle$  directions within the single-crystal approximation as  $E_{100} = (C_{11} + 2C_{12})(C_{11} - C_{12})/(C_{11} + C_{12})$  and  $E_{111} = \{1/E_{100} + (C_{11} - C_{12} - 2C_{44})/[3C_{44}(C_{11} - C_{12})]\}^{-1}$  and found a large anisotropy between  $E_{100}$  and  $E_{111}$ , which decreases with cobalt: the Young's modulus  $E_{100}$  increases from 140 to 168 GPa, while  $E_{111}$  decreases from 298 to 255 GPa with 6 at.% Co substitution.

In order to predict the shear and Young's moduli more accurately, we used the Voight–Reuss–Hill approach, where the single-crystal elastic constants are averaged to obtain the moduli for polycrystalline materials, which describe experimental results better than those obtained within the single-crystal approximation. The polycrystalline shear modulus calculated as  $G = (G_V + G_R)/2$ , where  $G_V = (C_{11} - C_{12} + 3C_{44})/5$  and  $G_R = 5(C_{11} - C_{12})(3C_{11} - 3C_{12} + 4C_{44})/C_{44}$ , is equal to 86 and 81 GPa for Fe and Fe–6 at.% Co, respectively. The

calculation of the Young's modulus as  $E = 9BG/(3B + G)$  shows a small decrease in  $E$  from 222 to 210 GPa with adding of 6 at.% Co.

Our calculated elastic moduli agree well with the experimental data for bcc Fe ( $B = 168$  GPa,  $G = 82$  GPa,  $E = 211$  GPa) [51] and theoretical prediction ( $B = 193.9$  GPa,  $G = 94.1$  GPa,  $E = 243.0$  GPa) [52] as well as with the trends predicted for random Fe–Co alloy [50], where the theoretical shear modulus and Young's modulus reduce by 8 and 3 %, respectively, upon 10 at.% Co substitution (our calculations predict the reduction of 6 and 5 % for 6 at.% Co). However, both theoretic predictions show an opposite trend with the available experimental data, where small positive slopes were detected for the shear and Young's moduli [53]. As discussed [50], these discrepancies may be related to the experimental measurements and/or the theoretic scheme of calculations (DFT approximation as well as the temperature and ordering effects). It can be suggested that the averaging method of single-crystal elastic constants may not describe the observed variation in moduli well enough—we found that with an addition of 6 at.% Co the shear modulus calculated within the single-crystal model increases by 24 %, while it decreases by 6 % within the polycrystalline model.

#### Cobalt on the (110) surfaces of bcc Fe and bcc Cu

In this section, we study the Co impurity substitution on the (110) surfaces of bcc Fe and bcc Cu. To model the (110) surface which corresponds to the lowest surface energy, we considered a supercell ( $10 \times 10 \times 6$   $k$ -mesh) consisting of 14 atomic layers separated by 10 Å of vacuum, and took into account the interlayer relaxation. Since we are going to study the Co behavior near the coherent interface between bcc phases of Fe and Cu, the calculations for the bcc Cu surface were performed by using the lattice parameter of bcc Fe.

We obtained the surface energy  $\gamma_s$  for the (110) plane in pure bcc Fe and bcc Cu to be 2.394 and 1.199 J/m<sup>2</sup>, respectively. Atomic relaxation of the topmost layers is very small in bcc Fe and has a negligible effect on the surface energy, while it decreases the surface energy of strained bcc Cu by 8 %, where the interlayer Cu–Cu distances strongly increase and approach to the values in unstrained bcc Cu. The calculated surface energies are in a good agreement with the experimental (averaged) value 2.360 J/m<sup>2</sup> [54] and with theoretical predictions 2.358 J/m<sup>2</sup> [55], 2.288 J/m<sup>2</sup> [56], and 2.43 J/m<sup>2</sup> [57] for the (110) plane in bcc Fe. In fcc Cu, the experimentally measured average surface energy and calculated surface energy for the (110) plane are equal to 1.49 J/m<sup>2</sup> [58] and 1.47 J/m<sup>2</sup> [59], respectively. We find that the surface energy calculated for the (110) plane in bcc Cu is close to the value for

fcc Cu as it was also found for the (110) planes in bcc Fe ( $\gamma_s = 2.358$  J/m<sup>2</sup>) and fcc Fe ( $\gamma_s = 2.380$  J/m<sup>2</sup>) [55]. Thus, much less energy is necessary for the formation of surface in bcc Cu that contributes to the precipitation of metastable bcc Cu particles—along with the strong attractive interaction between Cu atoms and the low solid solution solubility of Cu in bcc Fe.

The effect of cobalt on the (110) surface was examined by replacing of a half of atoms in the topmost layers of bcc Fe and bcc Cu. Cobalt in the topmost Fe layer causes the surface rippling with an amplitude of 0.06 Å and it is shifted inward relative to the surface Fe atoms. The Co–Fe distances for the first and second neighbors (2.38 and 2.78 Å, respectively) are less than the Fe–Fe distances in the bulk (2.46 and 2.83 Å), and cobalt forms strong bonds with the nearest Fe atoms. The magnetic moment of a surface cobalt atom increases only slightly from the bulk value 1.64  $\mu_B$  to 1.70  $\mu_B$ , whereas the nearest Fe atom in the surface layer has an enhanced magnetic moment of 2.81  $\mu_B$ , which is larger than the magnetic moment of the topmost Fe atoms (2.57  $\mu_B$ ) on the clean Fe surface. We found that Co atom on the bcc Cu surface ripples by 0.23 Å below the Cu atoms and has the same magnetic moment of 1.60  $\mu_B$  as in hcp Co. The shortest Co–Cu distance is 2.453 Å, while the distance between Cu atoms in the first and second layers (2.540 Å) is larger than those on the pure Cu surface (2.488 Å).

By cleaving the bcc Fe and Cu bulks along the Co-containing (110) plane, we obtained that the 50 % cobalt concentration in the topmost layer decreases the surface energy of bcc Fe by 0.086 J/m<sup>2</sup>, while it increases the surface energy of strained bcc Cu from 1.199 to 1.386 J/m<sup>2</sup>. Thus, we obtained that the Co-containing Fe surface is more favorable than the clean Fe surface due to the formation of strong Fe–Co bonds. Cobalt substitution on the Cu surface increases the surface energy of bcc Cu that can reduce the tendency for the formation of Cu precipitates and, hence, prevent their growth.

#### Cobalt effect on geometry and bonding in the Fe/Cu interface

We modeled the interphase region between the Fe matrix and Cu precipitate by the bcc Fe/bcc Cu interface which was constructed from bcc Fe and strained bcc Cu layers. Since the lattice mismatch between bcc Fe and bcc Cu is small, a coherent interface may be assumed for the bcc Fe/bcc Cu interface. The lateral lattice parameter of bcc Cu was adjusted to match the lattice constant of bcc Fe because Cu precipitates are small and soft. We studied the (110) bcc Fe/(110) bcc Cu interface, which was predicted to be more favorable than the (001) interface [15]. To simulate this interface, a 48-atom supercell was constructed from 8 Cu layers and 16 Fe layers with two atoms per

layer. During structure optimization, the lateral lattice parameter was accepted equal to that for bcc Fe, while the relaxation was allowed for all interlayer distances.

For clean Fe/Cu interface, the largest relaxation was obtained for atoms near the interfacial region. We found that near the interface the Fe–Fe and Cu–Cu layers are slightly compressed (Fe–Fe, Fe–Cu, and Cu–Cu distances are 2.435, 2.493, and 2.485 Å, respectively) as compared to the distances in equilibrium bcc Fe and Cu bulks (2.456 and 2.502 Å). The magnetic moment of the interfacial Fe atom ( $2.45 \mu_B$ ) is smaller than that of the topmost surface Fe atom ( $2.57 \mu_B$ ), whereas the bulk value is found in the third Fe layer below the interface.

We calculated the adhesion energy  $W_{ad}$  as the energy necessary for the interface separation into two free surfaces and obtained  $W_{ad} = 3317 \text{ mJ/m}^2$ . The interfacial energy  $\gamma_{\text{Fe/Cu}}$ , which represents the energy gain due to the interface formation, was calculated as  $\gamma_{\text{Fe/Cu}} = \gamma_{\text{Fe}} + \gamma_{\text{Cu}} - W_{ad}$ . We obtained  $\gamma_{\text{Fe/Cu}} = 276 \text{ mJ/m}^2$  that points to a weak interfacial bonding. Earlier MD simulations predicted a strong dependence of the interface energy on the size of Cu precipitate: 278 and  $1061 \text{ mJ/m}^2$  for spherical bcc precipitates of 2.3 nm and 4 nm in diameter [60], while  $\gamma_{\text{Fe/Cu}} = 207 \text{ mJ/m}^2$  was reported for Cu precipitate with a 4-nm diameter [15].

To determine the preferable cobalt positions in Fe/Cu, we used a 128-atom supercell consisting of six Cu layers and ten Fe layers with eight atoms per layer, and compared the cobalt substitutional sites in the middle of the Cu and Fe slabs as well as in the Cu and Fe layers near the interface. Earlier, it was established that the Cu precipitates contain Fe and its concentration may reach up to 33 % [39]. In order to understand how the Fe content in Cu cluster may affect the cobalt distribution, we compared the cobalt substitutions in the Fe/(Cu, Fe) interface with either a Cu slab composed only by Cu atoms (100 % Cu) or with the equal concentrations of Fe and Cu. In the latter case we used 48-atom supercell and ordered B2 structure for the Cu–Fe slab.

### Single cobalt impurity

For a single cobalt atom in the interface Fe layer, we found a rippling effect of 0.06 Å with Co below the Fe atoms in the first layer and a decrease in the interlayer Fe–Co distance to 1.942 Å. There is a small rippling amplitude in the next topmost Fe layers (0.01 Å), while amplitude in the topmost Cu layers is higher (0.06 Å) and it decreases slowly in the deeper layers. The magnetic moment of Co atom,  $1.61 \mu_B$ , is close to its value in the bulk, whereas the nearest Fe atom in the interface layer has magnetic moment of  $2.64 \mu_B$ . These values will be compared to those obtained for larger Co concentrations discussed below.

Table 1 shows the respective site preference energy  $E_{\text{pref}}$  for the substitution of one cobalt atom in a Fe or Cu layer (12.5 % Co per layer) of the Fe/(Cu, Fe) interface. Although the configuration with Co in the Fe matrix has the lowest energy (most preferred), while Co in Cu slab corresponds to the highest energy (least preferred) in each case considered, the difference between  $E_{\text{pref}}$  for Co in the Fe slab and in the Cu slab decreases by almost three times when the Fe concentration in Cu becomes 50 %. Furthermore, the presence of even a small concentration of Fe in the bcc Cu (4 % Fe) reduces  $E_{\text{pref}}$  for Co at the interface layers, weakening the tendency of Co to diffuse into the Fe matrix. Thus, we demonstrate that cobalt atom will move from the core of Cu precipitate, and this tendency is enhanced with a decrease of the Fe content in the Cu slab.

It is clear that a strong preference of cobalt to be in the Fe matrix is determined by the large difference in the mixing energies of the Co–Fe and Co–Cu alloys. As it is seen from the densities of states for Co atom at different locations in the Fe/Cu interface (Fig. 1), the filling of the Co 3*d* and Fe 3*d* states and their energy positions are very similar when Co is in the first interfacial Fe layer or in the middle of the Fe slab; this results in a small difference in their site preference energies (Table 1). In both cases, the Fermi level is located between the bonding and antibonding minority 3*d* states, while the majority 3*d* states are almost occupied. Compared to iron, cobalt has an additional valence electron, which spreads through the minority 3*d* states and strengthens the bonding and reduces its magnetic moment to  $1.7 \mu_B$  with respect to the iron moment ( $2.21 \mu_B$ ). We note, however, that when Co is in the first interfacial Fe layer, the Co 3*d* states are broadened and give a larger contribution near the Fermi level that indicates strengthening of Fe–Co bonds and explains why Co atom has no strong preference to be inside the Fe matrix (where Co has eight bonds with the nearest Fe atoms) or in the interfacial region (where Co has four Fe–Co bonds and four weak Fe–Cu bonds).

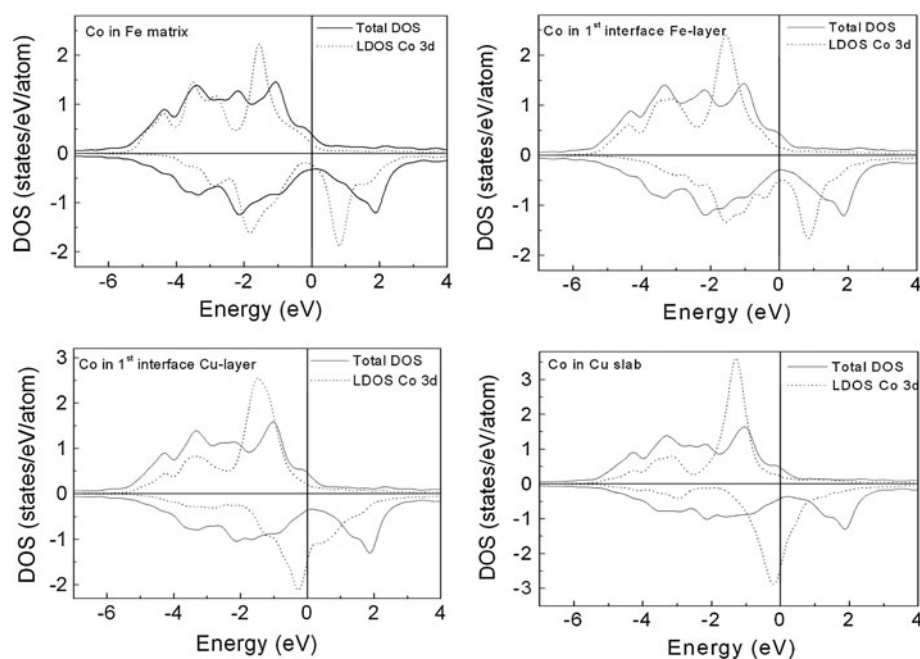
When Co occupies the Cu site in the first interfacial Cu layer or in the middle of Cu slab, the majority Co 3*d* states are also occupied, whereas the minority Co 3*d* states are shifted toward the higher energies, and the Fermi level falls at a sharp peak in the density of states. The Cu 3*d* states are filled and located much deeper than the Co 3*d* states. The Co 3*d*–Cu 3*d*, 4*s* hybridization is weak, and the minority Co 3*d* states are atomic-like and are not split into the bonding and antibonding states. For Co atom in the first interfacial Cu layer, where it has both Cu and Fe nearest neighbors, the interaction with the Fe 3*d* states broadens the Co 3*d* states, whereas for Co in the middle of Cu slab, the Co 3*d* peaks are narrow as for a spin-polarized atom. Because of the weak Co–Cu bonding, the site preference energy is much higher



**Table 1** Respective site preference energy  $E_{\text{pref}}$  (in eV) for the different positions of Co atom in the Fe/(Cu, Fe) interface with different Fe concentration in the Cu slab

Co site	Layer	100 % Cu	50 % Fe, 50 % Cu	4 % Fe, 96 % Cu
Co in Fe site	Fe slab	0	0	0
	Second layer	0	0	0
	First layer	0.08	0.02	0.03
Co in Cu site	First layer	0.22	0.14	0.09
	Second layer	0.63	0.19	0.34
	Cu slab	0.69	0.25	0.69

**Fig. 1** The total density of states for the Fe/Cu interface and the local total density of Co 3d states for different substitutional sites of Co. The positive and negative DOS correspond to the majority and minority states, respectively



for Co in 100 % Cu slab, but it decreases sharply due to the presence of Fe atoms in the Cu slab.

Although we found that the site preference energy for cobalt depends on the composition of the Cu slab, we note that the B2-like ordered Cu–Fe slab may not be a realistic model to describe the Fe distribution in Cu. To predict preferable iron positions in the Cu slab, we also calculated the total energies for the Fe/Cu interface with one Fe atom (12.5 % Fe per Cu layer) located in different Cu layers. We obtained that the most stable Fe site is in the first interface layer, whereas the substitutions in the second and third Cu layers have an energy higher by 0.37 and 0.44 eV, respectively. As it is seen from Table 1, the preferable Fe and Co distributions in the Cu slab are similar for both Fe and Co atoms—both prefer to occupy the interface layers. This means that during the formation of Cu particles from the Fe–Cu–Co solid solution, the iron content in Cu should decrease as the size of Cu particle increases. Hence, the Fe distribution in the Cu particle is not random, and both cobalt impurity and iron atoms prefer to move from the Cu core to the interfacial region. Because of the strong Fe–Co

bonds, one can expect their correlated behavior in the Cu particle.

Calculations for the Fe/Co/(Fe, Cu) interface with only two Fe atoms in the first interface Cu layer yield  $E_{\text{pref}}$  for Co in the middle of Cu slab to be the same as for 100 % Cu slab. However, much smaller values of  $E_{\text{pref}}$  were obtained for Co in the first and second Cu layers although the Fe content in Cu slab increased only slightly, 4 at.% Fe in Cu slab (Table 1). The energy difference between the Co sites in the Fe matrix and in the interface Fe layer also decreases when Fe atoms are present in the Cu particle. Thus, we believe that the presence of iron in copper particles even at low concentration, contributes to the appearance of cobalt in the interface region.

#### Cobalt segregation

Next, we consider the optimized geometry and stability of the Fe/Co/Cu interface for different Co concentrations in the interfacial Fe layer and in the Fe matrix. The effect of cobalt substitution on the stability of the Fe/Cu interface

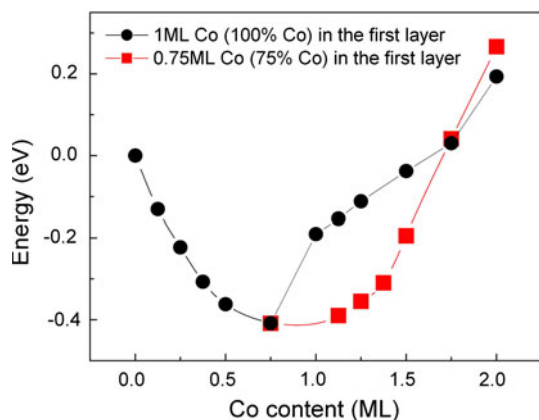


**Fig. 2** The energy gain  $E^{\text{int}}(\text{Co})$  as a function of Co concentration in the first and second interface Fe layers of (110) Fe/Cu. Circles correspond to the filling of the first interface layer (from 0.0 to 1.0 ML Co content per layer) followed by the consecutive filling of the second interfacial Fe layer with Co up to 100 % Co (2 ML Co). Squares represent incomplete first interfacial layer with 75 % (0.75 ML) Co concentration with the second Fe layer being filled up to 100 % Co (Color figure online)

was estimated as the energy gain  $E^{\text{int}}(\text{Co})$  for the formation of Fe/Co/Cu relative to pure Fe/Cu taking into account the difference in the Fe and Co bulk energies. We considered cobalt concentrations of 12.5 %, 25 %, 37.5 %, 50 %, 75 %, and 100 % in one or two Fe-interface layers, i.e., the Co content in the layers is varied from 0.125 to 2 ML, and found that cobalt with a concentration less than 1.75 ML in the interfacial region stabilizes the interface ( $E^{\text{int}}(\text{Co}) < 0$ ), Fig. 2. All Co atoms occupy bcc sites and the atomic relaxation within the lateral plane is small. The most stable configuration corresponds to 75 % Co (0.75 ML), and  $E^{\text{int}}(\text{Co})$  sharply increases by 0.2 eV when the interface layer is composed of only Co atoms (1 ML) although it is still negative. Furthermore, we find that Co substitutions in the second Fe layer give a lower energy for incomplete coverage, i.e., when the first layer contains 0.75 ML Co, but not 1 ML Co. The Fe/2 ML Co/Cu interface with two cobalt monolayers between the Fe and Cu slabs is highly unfavorable ( $E^{\text{int}}(\text{Co}) = +0.2$  eV, Fig. 2). It should be noted that the results of scanning tunneling microscopy and spectroscopy for Co films on the Fe (110) surface also showed that the ideal bcc structure of Co is stable only for the two topmost monolayers [61].

Similar to a single cobalt atom in the interface Fe layer, the rippling amplitude of 0.06 Å with Co below Fe atoms in the first layer was obtained for up to 100 % Co substitution in the interface Fe layer. We found that the smaller the cobalt content in the layer, the shorter the Fe–Co distance is. For 1 ML Co, the interlayer Co–Fe distance of 1.971 Å is shorter than those between the nearest Fe atoms near the (110) Fe/Cu interface (1.999 Å) as well as in the Fe bulk (2.005 Å).

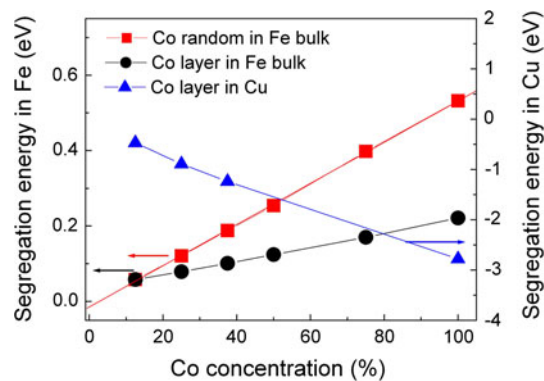


**Fig. 3** Interfacial cobalt segregation energy as a function of Co concentration in the layer of Fe/Cu with respect to the Co layer segregation in slab Fe (circles) and in slab Cu (triangles). Interfacial segregation energy of Co layer versus random distribution of Co in Fe bulk is also given (squares) (Color figure online)

Thus, the Co-containing interface is energetically more favorable than the free Fe/Cu interface due to the formation of the short and strong Fe–Co bonds near the interface. As demonstrated in “Single cobalt impurity” section, where one Co atom per layer (12.5 % Co in layer) is considered that cobalt has no strong preference to be in the Fe matrix (Table 1). In order to understand the effect of Co concentration, we calculated the interfacial segregation energy  $E^{\text{segr}}(\text{Co})$  as a total energy difference between the cobalt substitutions in the interface Fe layer and in the Fe slab. In both cases, we considered 1, 2, 3, 4, 6, and 8 Co atoms per one layer (either the first interfacial Fe layer or a layer within the Fe slab), which corresponds to 12.5 %, 25 %, 37.5 %, 50 %, 75 %, and 100 % Co concentration per layer, respectively. For comparison, we also calculated the bulk segregation energy—the difference between the energy of one Co layer in the Fe slab and of the random Co distribution in the Fe slab with the same Co concentration as in the layer. As expected, cobalt prefers to be randomly distributed in bcc Fe bulk and the bulk segregation energy (the difference between configurations with layer segregation in bulk and random distribution in bulk) sharply increases with Co concentration (Fig. 3).

We obtained that the interfacial segregation energy is positive when the Co concentration in the Fe layer is higher than 12.5 % and it increases linearly with Co concentration (Fig. 3). The linear fit of  $E^{\text{segr}}(\text{Co})$  shows that the energy is expected to remain positive for Co concentrations below 12.5 %. This suggests that the Co layer segregation in Fe slab is energetically preferable over the interface segregation, although the energy difference is rather small, ranging within 0.04–0.22 eV, Fig. 3. We found, however, that the interfacial segregation energy calculated with respect to random cobalt distribution in bulk Fe becomes negative,  $E^{\text{segr}}(\text{Co}) < 0$ , for concentration less than 2.4 at.% Co. This means that at the low concentration, cobalt prefers to

segregate in the interface layer—in agreement with our experimental observations [17]. It should be noted that the surface segregation energy for Co on the (110) Fe surface is known to have a small negative value [62, 63]. The Auger electron spectroscopy studies of surface segregation in Fe–Co alloys also demonstrated the maximum enrichment with cobalt at the surface in the alloy with minimum Co concentration [64].

Above, we stated that a single Co atom is rejected from the Cu precipitate and considered the cobalt segregation in the interfacial Fe layer and in the Fe matrix. However, the cobalt precipitates resulting in precipitation hardening have been observed in fcc (1.0–2.8 at.%) Co–Cu alloys [65, 66] and one can suggest their appearance in bcc Cu particles. Taking into account a possibility for cobalt clusters in bcc Cu, which was demonstrated in “Additions in bulk bcc Fe and bcc Cu” section, we now consider the preferable positions of cobalt dimer (25 % Co concentration in layer), trimer (37.5 % Co concentration in layer), as well as a Co monolayer (8 Co atoms or 100 % Co concentration in layer) in the Cu slab. First of all, we calculated the total energies of interfaces with the Co dimer inserted in the first, or second Cu layers or in the middle of the 100 % Cu slab and obtained that the first and the second interfacial layers are by 0.89 and 0.13 eV, respectively, more preferable for the Co dimer than its position in the middle of the Cu slab. We note that for a single Co atom, the energy difference between Co sites in the Cu slab and in the first Cu-interfacial layer is much smaller (0.47 eV for Fe/Cu interface, Table 1) than the above value of 0.89 eV for the Co dimer, suggesting that Co clusters are more likely to be rejected from the Cu core. Accordingly, the interfacial segregation energy  $E^{\text{segr}}(\text{Co})$  estimated as the total energy difference between cobalt substitutions in the interface Cu layer and in the Cu slab is a large negative value of  $-0.89$  eV for the Co dimer. The similar calculations for three Co atoms and Co monolayer in Cu yielded that  $E^{\text{segr}}(\text{Co})$  lowers with the number of Co atoms in the layer (Fig. 3). These calculations show that cobalt segregation is favorable in the topmost interface layer of Cu particle. Based on these results, we can suggest that Co is rejected from the Cu core and forms islands or a shell of the bcc Cu particles. It should be noted that the experimental [67] and theoretical [68, 69] studies also demonstrated the formation of compact Co clusters or islands on the fcc Cu surfaces.

Finally, we would like to understand how cobalt segregated on the surface of Cu particle affects its further growth. For this, we performed the total energy calculations for the Fe/Cu/Co and Fe/Cu/Co/Cu interfaces with the equal number of Cu monolayers. We found that the addition of a Cu monolayer above the Co monolayer sharply increases the energy by  $+0.634$  eV in comparison with the Fe/Cu/Co interface. This result demonstrates that the

presence of cobalt in a Cu particle makes adhesion of additional Cu atoms strongly unfavorable and inhibits the growth of Cu particle limiting its size.

### Cobalt-induced strengthening in Fe/Cu

The results of ab initio calculations predict that cobalt and iron atoms have a tendency to diffuse from the Cu core; hence, their concentration should decrease in the Cu precipitate during its formation from the solid Fe–Co–Cu solution. Moreover, cobalt on the surface of Cu particles prevents adhesion of additional Cu atoms that may slow down the growth of Cu particles. We predict that cobalt may segregate in the interfacial Cu layer as well as in the interfacial Fe layer for concentration below 2.4 at.% Co, but at higher concentrations cobalt atoms move into the Fe matrix.

These theoretical predictions explain the results of experimental studies of the Co-alloyed Cu precipitation hardened steel [16]. Previously [16, 17], we studied three bcc-based alloys with 0, 3, and 7 wt% Co and observed that Co addition increases the strength and toughness. By means of atom probe tomography, a decrease in Cu precipitate radius and a narrowed size distribution was observed with addition of Co. The concentration profile across the precipitate and the matrix reveals that the Co impurity was rejected from precipitate to matrix, in agreement with our theoretical prediction.

Now, we would like to determine a possible mechanism of cobalt-induced additional strengthening in Fe/Cu. Since cobalt is likely to be randomly distributed in the Fe matrix, it can be suggested that cobalt changes the dislocation mobility in bcc Fe. In order to understand the cobalt effect on the solid solution behavior, we calculated the GSF energies (which are closely related to the barrier for dislocation motion) as the total energy changes associated with a rigid shift of a one-half of the crystal at a fault vector  $\mathbf{u}$  along the  $\langle 111 \rangle$  direction in the (110) plane. A supercell was constructed from six  $\{110\}$  layers with eight atoms per layer, where the solute effect was modeled by substitution of one Fe atom on the slip plane. It corresponds to 12.5 at.% impurity in the shifted plane and 1.8 at.% impurity in bulk that is the maximum Cu solubility in bcc Fe at 850 °C [70].

The calculated GSF energy curves for the  $\langle 111 \rangle$  (110) slip are shown in Fig. 4 for ferromagnetic bcc Fe, bcc Fe–1.8 at.% Cu, and Fe–1.8 at.% Co solid solutions. For ferromagnetic bcc Fe, we obtained the maximum GSF energy  $\gamma_{\text{us}} = 0.52$  J/m<sup>2</sup> at  $1/2\langle 111 \rangle$  (110) displacement to be in a good agreement with the previous calculations, 0.59 and 0.47 J/m<sup>2</sup> in spin-polarized LDA and GGA calculations, respectively [71], as well as with atomistic predictions of 0.60–0.89 J/m<sup>2</sup> as dependent on the Fe potential [72, 73]. For non-magnetic bcc Fe, we obtained the negative GSF



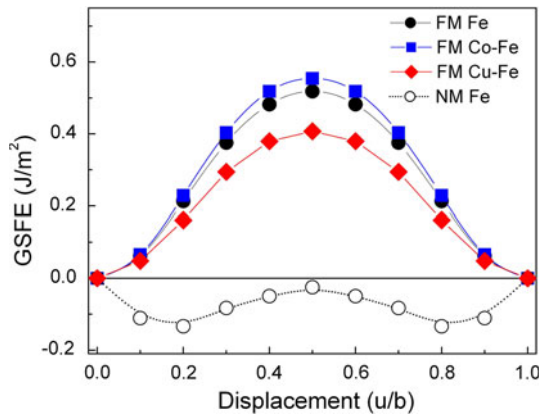


**Fig. 4** GSF energies for  $u \langle 111 \rangle (110)$  slip in bcc Fe, bcc Fe–Cu, and Fe–Co solid solutions (Color figure online)

energies for all displacements and this unphysical result can be explained by the fact that non-magnetic bcc Fe has a much higher energy than the other Fe phases [43]. Therefore, we conclude that magnetism plays a crucial role in sliding and may affect the dislocation in bcc Fe.

The Co atom inserted on the sliding (110) plane changes  $\gamma_{us}$  only insignificantly ( $0.56 \text{ J/m}^2$ ). Taking into account that the atomic sizes and shear moduli are close, it can be concluded that cobalt at low concentration and low temperature produces neither solid solution softening nor hardening which would originate from a size/modulus mismatch between the solute and solvent atoms. The Cu atom substituted for Fe on the sliding plane decreases  $\gamma_{us}$  to  $0.40 \text{ J/m}^2$  in Fe–1.8 % Cu, and Cu addition is expected to lead to a solid solution softening in bcc Fe. The results of atomic row modeling also demonstrated that Cu solutes in bcc Fe act as lubricants and facilitate the Fe–Cu shear process due to weak Fe  $3d$ –Cu  $4s$  bonding [32].

We demonstrated above that cobalt may segregate at the interface between the Fe matrix and Cu precipitates and forms strong Fe–Co bonds near the interface. The enhanced bonding in the interfacial region may provide an additional strengthening effect. In order to simulate the cobalt strengthening effect, we calculated the ideal cleavage energies and the critical cleavage stress for a fracture between different interfacial layers. These brittle cleavage parameters describe the crack formation and help to predict the habit fracture planes as well as to explain the trends in hardness [74]. Although the calculated ideal cleavage energy and stress are known to overestimate the observed values, they provide their upper limit which is determined by the strength of chemical bonds.

We modeled the cleavage process by varying the separation  $x$  between slabs stacked along the  $z$  axis. The asymptotic value of the total energy change  $G_c(x)$  determines the ideal cleavage energy  $G_c$ , whereas the maximum derivative  $\sigma(x) = \partial G_c / \partial x$  defines the critical cleavage

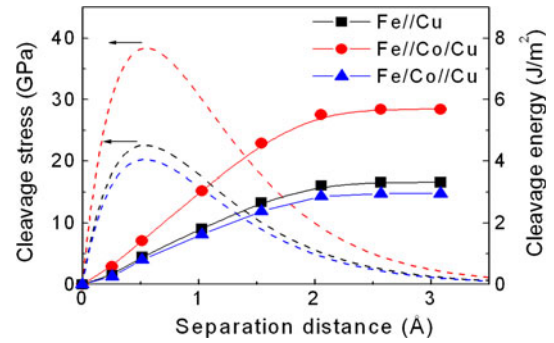


**Fig. 5** Cleavage energy  $G_c(x)$  and stress  $\sigma(x)$  as dependent on separation  $x$  for clean Fe/Cu and Fe/Co/Cu with Co monolayer. Fe//Co/Cu and Fe/Co//Cu denote the cleavage between Fe and Co layers and between the Co and Cu layers, respectively. The equilibrium interlayer distances correspond to  $x = 0$  (Color figure online)

stress  $\sigma_c$ . By calculating  $G_c$  for the interface as its separation into two free surfaces, we estimated the energy required to break the interfacial bonds. By means of the universal binding energy relation [75], we also determined the critical length  $\ell$  corresponding to  $\sigma(x) = \sigma_c$ .

For the clean Fe/Cu interface, the cleavage energy (adhesion energy) is equal to  $3.32 \text{ J/m}^2$  and  $\sigma_c \approx 22 \text{ GPa}$  (Fig. 5). With the Co monolayer present between the Fe and Cu slabs, we considered two cleavage (110) planes between the Co and Fe layers or between the Co and Cu layers. For cleavage between the Co and Cu layers, we obtained that  $G_c$  ( $2.96 \text{ J/m}^2$ ) and  $\sigma_c$  ( $20 \text{ GPa}$ ) are close to those between the Fe and Cu layers in the clean Fe/Cu interface. The values are twice larger ( $5.86 \text{ J/m}^2$  and  $38 \text{ GPa}$ , respectively) for cleavage between the Co and Fe layers. The critical length  $\ell$  is  $0.53$  and  $0.51 \text{ \AA}$  for both cleavage planes. Thus, we predict that the interfacial interaction between the Co and Cu layers is almost the same as between the Fe and Cu layers in the Fe/Cu interface, whereas it sharply increases between the Co and Fe layers in the Fe/Co/Cu interface. We demonstrated that cobalt increases the bonding strength near the interface between the Fe matrix and Cu particle, and the lattice resistance in the [110] direction should increase. The compressive stress which arises near the interface due to the strong and short Fe–Co bonds may serve as a barrier for dislocations.

### Summary

By means of ab initio method, we investigated the cobalt effect in bulks and at the surfaces of bcc Fe and bcc Cu, as well as in the Fe/Cu interface. Cobalt in bcc Fe bulk does not change the elastic moduli and does not produce a solid solution softening or hardening. We predicted the cobalt distribution between the Fe matrix and the Cu precipitate as well as the cobalt effect on the interfacial bonding. Both cobalt and iron are present in the Cu precipitates at early stages of aging (i.e. when the Cu

precipitates are nucleated from solid solution), but when the bcc Cu structure is formed, they diffuse from the core of Cu precipitate. The adhesion of Cu atoms is prevented when cobalt segregates on the surface of Cu particle, which slows further growth of Cu particles. Cobalt, which is likely to appear in the interfacial region as islands or a shell of Cu particle, forms strong Fe–Co bonds, which increase the cleavage stress and the lattice resistance to crack propagation. This strengthening effect is similar to precipitation hardening and the Co shell with strong bonding in the interfacial region may serve as an obstacle for dislocation motion and may increase the hardness of bcc Fe with Cu precipitates.

## References

- Russell KC, Brown LM (1972) *Acta Metall* 20:969
- Harry T, Bacon DJ (2002) *Acta Mater* 50:195
- Harry T, Bacon DJ (2002) *Acta Mater* 50:209
- Fine ME, Isheim D (2005) *Scr Mater* 53:115
- Liu J, van Walle A, Ghosh G, Asta MD (2005) *Phys Rev B* 72:144109
- Fine ME, Liu JZ, Asta MD (2007) *Mater Sci Eng A* 463:271
- Bacon DJ, Osetsky YN (2009) *Philos Mag* 89:3333
- Nedelcu S, Kizler P, Schmauder S, Moldovan N (2000) *Model Simul Mater Sci Eng* 8:181
- Marian J, Wirth BD, Schaublin R, Odette GR, Perlado JM (2003) *J Nucl Mater* 323:181
- Osetsky YN, Bacon DJ, Mohles V (2003) *Philos Mag* 83:3623
- Kohler C, Kizler P, Schmauder S (2005) *Model Simul Mater Sci Eng* 13:35
- Topasa K, Bacon DJ, Osetsky YN (2006) *Model Simul Mater Sci Eng* 44:1153
- Shim JH, Kim DI, Jung WS, Cho YW, Hong KT, Wirth BD (2008) *J Appl Phys* 104:083523
- Karkin IN, Gornostyrev YN, Karkina LE (2010) *Rev Adv Mater Sci* 25:164
- Ludwig M, Farkas D, Pedraza D, Schmauder S (1998) *Model Simul Mater Sci Eng* 6:19
- Murthy AS, Lekakh S, Van Richards VL, Van Aken D (2011) Proceedings of symposia held during the TMS annual meeting and exhibition, 2011. Wiley, Hoboken, p 651
- Murthy AS, Medvedeva JE, Isheim D, Lekakh S, Richards VL, Van Aken DC (2012) *Scr Mater* 66:943
- Maury F, Lorenzelli N, De Novion CH (1991) *J Nucl Mater* 183:217
- Koyama T (2008) *AMTC Lett Jpn Fine Ceram Cent* 1:817
- Isheim D, Gagliano MS, Fine ME, Seidman DN (2006) *Acta Mater* 54:841
- Miller MK, Russell KF (2007) *J Nucl Mater* 371:145
- Pareige PJ, Russell KF, Miller MK (1996) *Appl Surf Sci* 94/95:362
- Srinivas M, Malakondaiah G, Rama Rao P (1988) *Bull Mater Sci* 11:329
- Stephens RJ, Witzke WR (1976) *J Less Common Met* 48:285
- Spitzig WA, Leslie WC (1971) *Acta Metall* 19:1143
- Okazaki K (1995) *J Mater Sci* 31:1087. doi:10.1007/BF00352911
- Chen L, Qiu Z (2007) *Defect Diffus Forum* V261–262:37
- Suzuki H (1979) In: Nabarro FRN (ed) *Dislocations in solids*, vol 4. North-Holland, Amsterdam
- Medvedeva NI, Gornostyrev YN, Freeman AJ (2005) *Phys Rev Lett* 94:136402
- Medvedeva NI, Gornostyrev YN, Freeman AJ (2005) *Phys Rev B* 72:134107
- Trinkle DR, Woodward C (2005) *Science* 310:1665
- Chen Z, Kioussis N, Ghoniem N, Hasebe T (2008) *Phys Rev B* 77:014103
- Vitek V (1968) *Philos Mag* 18:773
- Mitchell TE, Anderson PM, Baskes MI, Chen SP, Hoagl RG, Misra A (2003) *Philos Mag* 83:1329
- Medvedeva NI, Gornostyrev YN, Freeman AJ (2007) *Phys Rev B* 76:212104
- Zhao D, Zhou L, Kong Y et al (2011) *J Mater Sci* 46:7839. doi:10.1007/s10853-011-5765-4
- Othen PJ, Jenkins ML, Smith GDW (1994) *Philos Mag A* 70:1
- Goodman SR, Brenner SS, Low JR Jr (1973) *Met Trans* 4:2363
- Isheim D, Seidman DN (2004) *Surf Interface Anal* 36:569
- Kresse G, Furthmuller J (1996) *Phys Rev B* 54:11169
- Kresse G, Hafner J (1996) *J Phys Condens Matter* 6:8245
- Perdew JP, Burke K, Ernzerhof M (1996) *Phys Rev Lett* 77:3865
- Herper HC, Hoffmann E, Entel P (1999) *Phys Rev B* 60:3839
- Kraft T, Marcus PM, Methfessel M, Scheffler MT (1993) *Phys Rev B* 48:5886
- Osetsky YN, Serra A (1997) *Philos Mag* 75:1097
- Soisson F, Fu CC (2007) *Phys Rev B* 76:214102
- Ackland GJ, Bacon DJ, Calder AF, Harry T (1997) *Philos Mag* 75:713
- Schmidt C, Ernst F, Finnis MW, Vitek V (1995) *Phys Rev Lett* 75:2160
- Gorbatov OI, Ruban AV, Korzhavyi PA, Gornostyrev YN (2009) *Mater Res Soc Symp Proc* 1193:469
- Zhang H, Punkkinen MP, Johansson B, Vitos L (2010) *J Phys Condens Matter* 22:275402
- Kittel C (1996) *Introduction to solid state physics*, 7th edn. Wiley, New York
- Zhang HL, Johansson B, Vitos L (2009) *Phys Rev B* 79:224201
- Speich GR, Schwoeble AJ, Leslie WC (1972) *Metall Trans* 3:2031
- Tyson WR, Miller WA (1977) *Surf Sci* 62:267
- Chamati H, Papanicolaou NI, Mishin Y, Papaconstantopoulos DA (2006) *Surf Sci* 600:1793
- Arya A, Carter E (2003) *J Chem Phys* 118:8982
- Vitos L, Ruban AV, Skriver HL, Kollár J (1998) *Surf Sci* 411:186
- Bauer CE, Speiser R, Hirth JP (1976) *Metall Mater Trans A* 7:75
- Mishin Y, Mehl MJ, Papaconstantopoulos DA, Voter AF, Kress JD (2001) *Phys Rev B* 63:224106
- Osetsky YN, Serra A (1996) *Philos Mag A* 73:249
- Methfessel T, Elmersm HJ (2009) *Surf Sci* 603:462
- Ruban A, Skriver H, Nørskov J (1999) *Phys Rev B* 59:15990
- Christensen A, Ruban AV, Stoltze P, Jacobsen KW, Skriver HL, Nørskov JK, Besenbacher F (1997) *Phys Rev B* 56:5822
- Jain NC, Kumar L (1989) *Appl Surf Sci* 40:223
- Hummel RE, Goho WM, Gerold V (1988) *Phys Status Solidi (a)* 106:641
- Takeda M, Inukai K, Suzuki N, Shinohara G, Hashimoto H (1996) *Phys Status Solidi (a)* 158:39
- Kief MT, Egelhoff WF (1993) *Phys Rev B* 47:10785
- Pentcheva R, Scheffler M (2000) *Phys Rev B* 61:2211
- Borisova SD, Ereemeev SV, Rusina GG, Stepanyuk VS, Bruno P, Chulkov EV (2008) *Phys Rev B* 78:075428
- Salje G, Feller-Kniepmeier M (1977) *J Appl Phys* 48:1833
- Yan JA, Wang CY, Wang SY (2004) *Phys Rev B* 70:174105
- Mishin Y, Mehl MJ, Papaconstantopoulos DA (2005) *Acta Mater* 53:4029
- Peter PA, Gordon A, Neeraj T, Luton MJ, Farkas D (2007) *Metall Mater Trans A* 38:2191
- Lazar P, Podlucky R (2008) *Phys Rev B* 78:104114
- Rose JH, Smith JR, Ferrante J (1983) *Phys Rev B* 28:1835